nature genetics

Germline loss-of-function mutations in *LZTR1* predispose to an inherited disorder of multiple schwannomas

Arkadiusz Piotrowski[1,2,15], Jing Xie[1,15], Ying F Liu[1], Andrzej B Poplawski[1], Alicia R Gomes[1], Piotr Madanecki[2], Chuanhua Fu[1], Michael R Crowley[3], David K Crossman[3], Linlea Armstrong[4], Dusica Babovic-Vuksanovic[5], Amanda Bergner[6], Jaishri O Blakeley[6], Andrea L Blumenthal[7], Molly S Daniels[8], Howard Feit[9], Kathy Gardner[10], Stephanie Hurst[7], Christine Kobelka[11], Chung Lee[12], Rebecca Nagy[13], Katherine A Rauen[12], John M Slopis[14], Pim Suwannarat[11], Judith A Westman[13], Andrea Zanko[12], Bruce R Korf[1,3] & Ludwine M Messiaen[1]

Constitutional *SMARCB1* mutations at 22q11.23 have been found in ~50% of familial and <10% of sporadic schwannomatosis cases[1]. We sequenced highly conserved regions along 22q from eight individuals with schwannomatosis whose schwannomas involved somatic loss of one copy of 22q, encompassing *SMARCB1* and *NF2*, with a different somatic mutation of the other *NF2* allele in every schwannoma but no mutation of the remaining *SMARCB1* allele in blood and tumor samples. *LZTR1* germline mutations were identified in seven of the eight cases. *LZTR1* sequencing in 12 further cases with the same molecular signature identified 9 additional germline mutations. Loss of heterozygosity with retention of an *LZTR1* mutation was present in all 25 schwannomas studied. Mutations segregated with disease in all available affected first-degree relatives, although four asymptomatic parents also carried an *LZTR1* mutation. Our findings identify *LZTR1* as a gene predisposing to an autosomal dominant inherited disorder of multiple schwannomas in ~80% of 22q-related schwannomatosis cases lacking mutation in *SMARCB1*.

Schwannomatosis (MIM 162091), the third major form of neurofibromatosis, is a late-onset tumor predisposition disorder that is clinically and genetically distinct from neurofibromatosis types 1 (MIM 162200) and 2 (MIM 101000). Although isolated schwannomas are common benign tumors, schwannomatosis—characterized by the development of multiple schwannomas without the bilateral vestibular schwannomas, congenital cataracts or ependymomas typically associated with neurofibromatosis type 2—is rare; however, its exact incidence is unknown[2,3]. While constitutional *NF2* mutations are not found, independent somatic mutations affecting both *NF2* alleles are typically present in every schwannoma of individuals with schwannomatosis[4]. Multipoint linkage analysis in families with schwannomatosis pointed to an ~8.48-Mb region centromeric to the *NF2* locus, between markers D22S420 and D22S1148, as the linked region[5]. Germline mutations in *SMARCB1*, located in this region and previously known to cause rhabdoid tumor predisposition syndrome (RTPS), have since been found in schwannomatosis cases[2,6–10]. Genetic analysis of schwannomas in cases with a *SMARCB1* germline mutation (first event, E1) shows loss of a region at 22q (second event, E2), with retention of the *SMARCB1* mutation in the schwannomas, followed by mutation of the remaining wild-type *NF2* gene (third event, E3) in *cis* with the *SMARCB1* germline mutation[2,7]. These three events result in biallelic loss of both the *SMARCB1* and *NF2* tumor suppressor genes in the schwannomas.

As germline *SMARCB1* mutations account for only ~50% of familial and <10% of sporadic cases[11], additional schwannomatosis-predisposing loci probably exist. A subset of cases had no constitutional first-hit *SMARCB1* mutation but had deletion of part of 22q encompassing both *NF2* and *SMARCB1* and somatic mutation of the remaining *NF2* allele in the schwannomas (Online Methods and **Supplementary Fig. 1**). We hypothesized that either functionally important sequences outside of the *SMARCB1* regions previously analyzed through clinical testing (for example, introns, 5′ or 3′ UTRs or intergenic regions) or an alternative evolutionarily conserved locus on chromosome 22 might carry a first hit predisposing to

[1]Medical Genomics Laboratory, Department of Genetics, University of Alabama at Birmingham, Birmingham, Alabama, USA. [2]Faculty of Pharmacy, Medical University of Gdansk, Gdansk, Poland. [3]Heflin Center for Genomic Sciences, University of Alabama at Birmingham, Birmingham, Alabama, USA. [4]Department of Medical Genetics, University of British Columbia, Vancouver, British Columbia, Canada. [5]Department of Medical Genetics, Mayo Clinic College of Medicine, Rochester, Minnesota, USA. [6]Johns Hopkins Comprehensive Neurofibromatosis Center, Baltimore, Maryland, USA. [7]Lakeridge Health Corporation, Oshawa, Ontario, Canada. [8]Clinical Cancer Genetics Program, MD Anderson Cancer Center, University of Texas, Houston, Texas, USA. [9]Department of Neurology, Henry Ford Hospital, Detroit, Michigan, USA. [10]Department of Neurology, Veterans Administration Hospital of Pittsburgh and University of Pittsburgh, Pittsburgh, Pennsylvania, USA. [11]Kaiser Permanente Genetics Northern California, San Francisco, California, USA. [12]Department of Pediatrics, Division of Medical Genetics, University of California, San Francisco, San Francisco, California, USA. [13]Department of Internal Medicine, Division of Human Genetics, Ohio State University Wexner Medical Center, Columbus, Ohio, USA. [14]Department of Neuro-Oncology, MD Anderson Cancer Center, University of Texas, Houston, Texas, USA. [15]These authors contributed equally to this work. Correspondence should be addressed to L.M.M. (lmessiaen@uabmc.edu).

Received 31 May; accepted 2 December; published online 22 December 2013; doi:10.1038/ng.2855

Table 1 ***LZTR1*** **mutations identified in 16 unrelated schwannomatosis cases**

Subject	Genomic position[a]	Genomic mutation	Exon or intron	cDNA mutation (blood)	Protein alteration	Type of mutation	Predicted effect of missense mutation			ESP allele[b]
							PolyPhen	SIFT	MutationTaster	
S3	Chr. 22: 21336687	c.27delG[c]	E1	–	p.Gln10Argfs*15	Truncating	NA	NA	NA	G = 12,702
S2	Chr. 22: 21337353	c.238dupA	E2	r.238dupa	p.Ile80Asnfs*15	Truncating	NA	NA	NA	A = 13,006
NGS2	Chr. 22: 21340117	c.264–13G>A[c]	IVS2	r.263_264ins264–11_264–1	p.Lys89Cysfs*16	Truncating, out-of-frame splice site	NA	NA	NA	G = 13,006
NGS3	Chr. 22: 21341837	c.365C>T[c]	E4	–	p.Ser122Leu	Missense	Probably damaging (1.00)	Deleterious (0.00)	Disease causing (probability = 1.0)	C = 13,006
S7	Chr. 22: 21343911	c.594–3C>G[c]	IVS6	r.594_651del (skip E7)	p.Leu199Trpfs*34	Truncating/ out-of-frame splice	NA	NA	NA	C = 12,998, T = 8[f]
S5	Chr. 22: 21347143	c.1210G>A	E11	–	p.Gly404Arg	Missense	Probably damaging (0.999)	Deleterious (0.01)	Disease causing (probability = 1.0)	G = 13,000
NGS8	Chr. 22: 21348226	c.1367T>G	E13	r.1367u>g	p.Val456Gly	Missense	Probably damaging (0.97)	Deleterious (0.00)	Disease causing (probability = 1.0)	T = 13,006
S9	Chr. 22: 21348256	c.1397G>A[c]	E13	–	p.Arg466Gln	Missense	Probably damaging (1.00)	Deleterious (0.00)	Disease causing (probability = 1.0)	G = 13,002
NGS6	Chr. 22: 21348309	c.1449+1G>A	IVS13	r.1354_1449del (skip E13)	p.Glu453_Lys484del	32-residue deletion, in-frame splice site	NA	NA	NA	G = 12,984
NGS5	Chr. 22: 21348502	c.1559C>T[c]	E14	–	p.Pro520Leu	Missense	Probably damaging (0.98)	Deleterious (0.02)	Disease causing (probability = 1.0)	C = 12,978
S8	Chr. 22: 21348982	c.1751dupA	E15	–	p.Ser585Glufs*84	Truncating	NA	NA	NA	A = 13,004
NGS7	Chr. 22: 21350154	c.2062C>T[c,d]	E17	r.2062c>u	p.Arg688Cys	Missense	Probably damaging (1.00)	Deleterious (0.00)	Disease causing (probability = 1.0)	C = 13,002
S4	Chr. 22: 21350154	c.2062C>T[d]	E17	–	p.Arg688Cys	Missense	Probably damaging (1.00)	Deleterious (0.00)	Disease causing (probability = 1.0)	C = 13,002
NGS1	Chr. 22: 21350969	c.2220–16_2220–14delCTT	IVS18	r. =	p. = ?[e]	Splicing?	NA	NA	NA	C,T,T = 13,006
S6	Chr. 22: 21351197	c.2348_2351delCGCA[c]	E20	–	p.Thr783Argfs*5	Truncating	NA	NA	NA	C = 13,005; T = 1; G,C,A = 13,006[g]
S1	Chr. 22: 21351552	c.2438G>T[c]	E21	r.2438g>u	p.Ser813Ile	Missense	Probably damaging (0.996)	Deleterious (0.01)	Disease causing (probability = 1.0)	G = 13,006

None of the mutations was present in dbSNP137, 1000 Genomes Project Phase 1 integrated release variations or the National Heart, Lung, and Blood Institute (NHLBI) GO Exome Sequencing Project (ESP) Exome Variant Server v.0.0.21 (August 2013). A prefix of "NGS" indicates samples included in the next-generation sequencing cohort, and a prefix of "S" indicates, samples included in the Sanger sequencing cohort. Chr., chromosome; –, not tested; IVS, intron; E, exon, NA, not applicable.

[a]Genomic positions are given according to the hg19 reference assembly. Reference transcript (hg19) is available under accession NM_006767.3. [b]Allele counts are according to the NHLBI GO ESP Exome Variant Server (v.0.0.18; accessed 8 February 2013). [c]Mutations were also found in relatives available for targeted *LZTR1* mutation analysis (see **Fig. 3**). [d]A recurrent mutation found in two unrelated cases. [e]Likely pathogenic mutation affecting the highly evolutionarily conserved CTT nucleotide motif within the splice acceptor of exon 19: phastCons score of 1.00 and phyloP score for the consecutive nucleotides of 2.87, 2.95 and 2.14. [f]The c.594–3C>T transition is annotated in ESP but is predicted not to affect splicing, whereas the c.594–3C>G transversion has not previously been reported. c.594–3C>G is predicted to create a novel splice acceptor sequence and to decrease the strength of the wild-type splice acceptor site, and it was proven in this study to cause aberrant splicing (skipping of exon 7) at the mRNA (cDNA) level. [g]c.2348C>T is a SNP (rs143507674) at chr. 22: 21,351,197 in dbSNP137; however, no pathogenic c.2348_2351delCGCA is present in dbSNP137 or ESP.

schwannomatosis in these cases. Here we report studies of germline DNA in 20 unrelated probands (6 familial cases, 11 sporadic cases and 3 cases with unknown family history of schwannomatosis; **Supplementary Table 1**) with an unknown first-hit mutation in blood and schwannomas (E1?), loss of 22q ($E2^+$) and a different *NF2* mutation in every schwannoma ($E3^+$) (**Supplementary Fig. 1**). We selectively enriched for 3.72 Mb of highly conserved sequence along chromosome 22 and initially performed deep parallel sequencing in eight cases (NGS1–NGS8) (**Table 1** and Online Methods).

Variants were called with Platypus and SVDetect[12], which, in addition to identifying germline mutations, includes a search for mosaic and structural variants. Initial filtering identified a single gene, *LZTR1*, carrying previously unreported exonic nonsynonymous variants in four of eight cases (**Supplementary Table 2**); these variants encoded p.Ser122Leu, p.Val456Gly, p.Pro520Leu and p.Arg688Cys alterations, all of which are missense changes affecting highly conserved amino acids and are predicted *in silico* to be damaging (**Figs. 1** and **2**, **Table 1**, **Supplementary Fig. 2** and **Supplementary Tables 3** and **4a**). Manual examination of intronic *LZTR1* sequences identified mutations affecting conserved splice sites in three additional probands of this initial cohort; these mutations included c.264–13G>A, c.1449+1G>A and c.2220–16_2220–14delCTT (**Supplementary Fig. 3**). All mutations were confirmed by Sanger sequencing. Analysis of discrepancies in insert size and anomalies in mapping information did not identify likely pathogenic intrachromosomal changes (Online Methods and **Supplementary Table 5**).

Sanger sequencing of *LZTR1* in lymphocyte DNA from 12 further unrelated $E1?E2^+E3^+$ probands (S1–S12) identified additional mutations in 9 cases (**Fig. 1** and **Table 1**). In total, 15 different previously unreported germline mutations in *LZTR1* were found in 16 of 20 unrelated schwannomatosis probands negative for *SMARCB1* mutation ($E1?E2^+E3^+$) but in 0 of 8 schwannomatosis probands positive for *SMARCB1* mutation ($E1^+E2^+E3^+$) ($P = 0.0002$, two-tailed

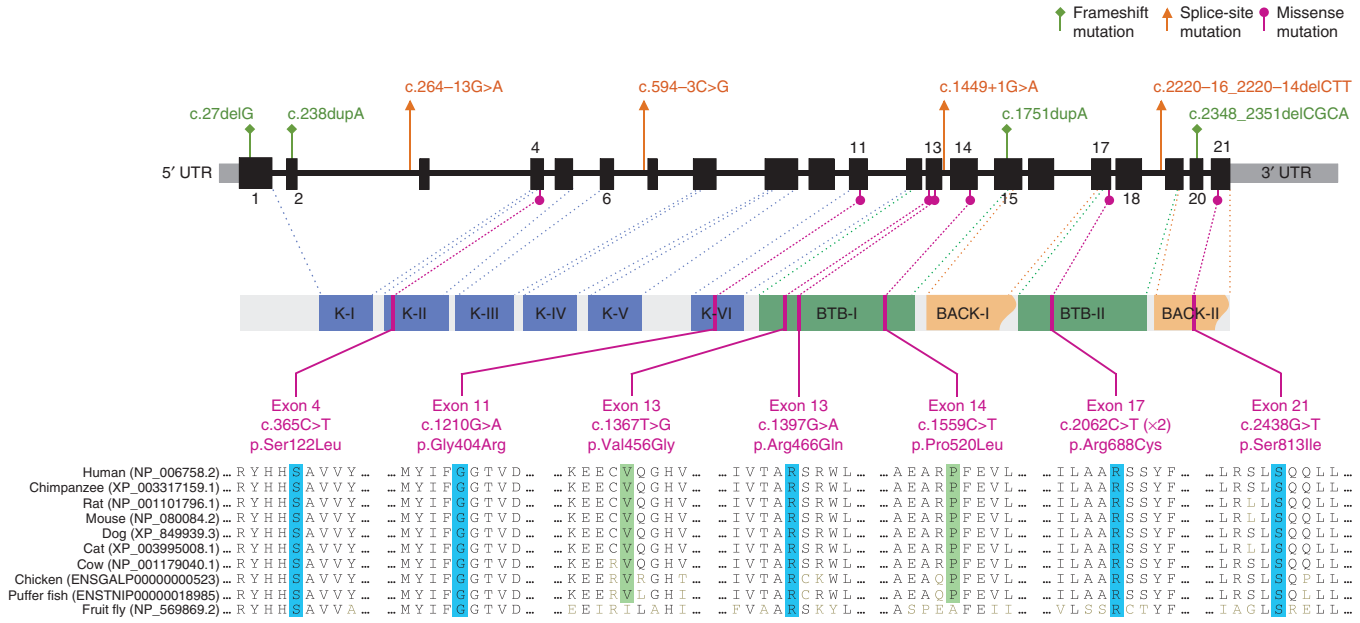

Figure 1 Distribution of mutations identified in the *LZTR1* gene in individuals with schwannomatosis. Top, locations of frameshift, splice-site and missense mutations. Exons, introns and 5′ and 3′ UTRs are indicated by thick, thin and gray segments, respectively. Middle, LZTR1 protein domains and the locations of the genomic sequences encoding them (dotted lines): K-I–K-VI, Kelch motifs of the Kelch domain; BTB-I and BTB-II, BACK-I and BACK-II (partial BACK) domains. Bottom, missense mutations and the evolutionary conservation of the affected amino acids across ten different species up to the fruit fly. Blue, amino acids conserved up to the fruit fly; green, amino acids conserved up to the puffer fish. Recurrent p.Arg688Cys alterations were found in two unrelated individuals. An accession code for the GenBank protein record is given in parentheses for each species. See also **Table 1**.

Fisher's exact test; **Supplementary Table 6**), including 6 truncating mutations (4 frameshift and 2 out-of-frame splice-site mutations), 1 in-frame splice-site mutation, a 3-nt deletion affecting a highly evolutionarily conserved splice acceptor sequence and 7 different missense mutations predicted to be damaging, all of which were absent in dbSNP137, the 1000 Genomes Project and ESP6500 (**Fig. 1**, **Table 1**, **Supplementary Figs. 2–4** and **Supplementary Table 4**). The spectrum of mutations suggests that loss of function is the main mechanism. *LZTR1*, located at 22q11.21, contains 21 exons and generates multiple alternatively spliced transcripts, with the longest ORF encoding an 840-residue protein[13]. *LZTR1* is expressed ubiquitously and abundantly in human tissues[13,14]. *LZTR1* resides centromeric to *SMARCB1*, also within the previously identified schwannomatosis-associated linkage interval[5]. Loss of heterozygosity with retention of the case-specific *LZTR1* mutation was found in all 25 schwannomas studied, strongly supporting the hypothesis that the *LZTR1* mutations are pathogenic (the likelihood of such genetic changes occurring by chance in all 25 tumors in 16 unrelated cases is conservatively ~1.5×10^{-5}) and consistent with a tumor suppressor mode of action for *LZTR1* (**Supplementary Figs. 1** and **5**). The *LZTR1* mutations segregated

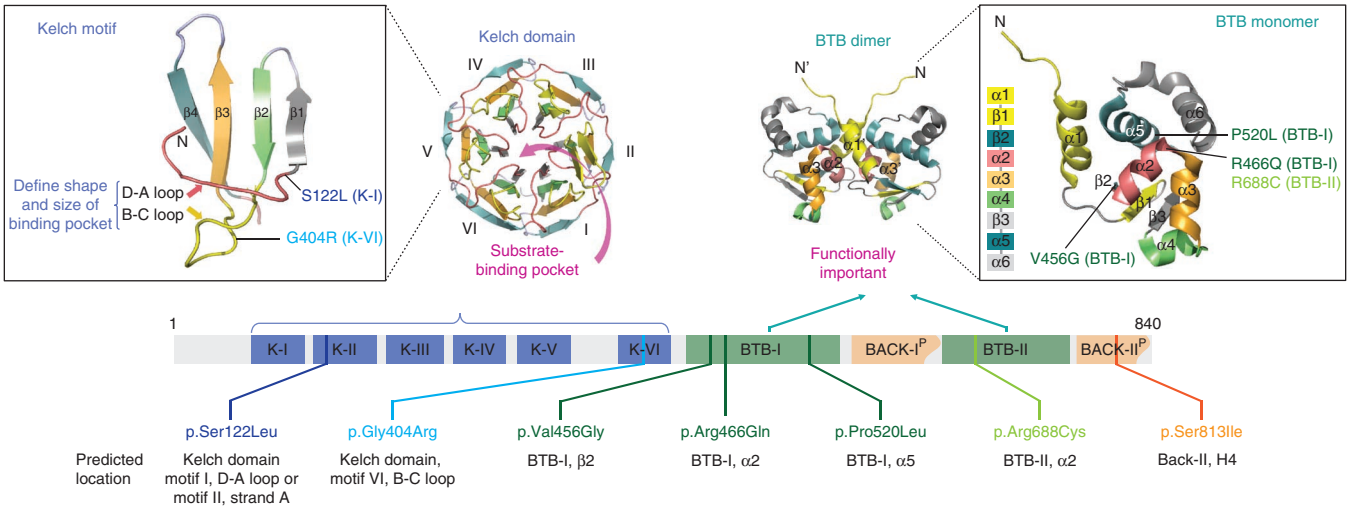

Figure 2 Structural domains of LZTR1 and spatial predictions for missense alterations. Top left, structural modeling of a single Kelch motif and the predicted locations of missense alterations, as well as the entire Kelch domain consisting of six Kelch motifs (K-I to K-VI). Top right, structural modeling of dimeric and monomeric BTB domains (along with sequential distribution of α helices and β sheets) and the predicted locations of missense alterations in the BTB-I and BTB-II domains. Bottom, distribution and predicted locations of missense alterations.

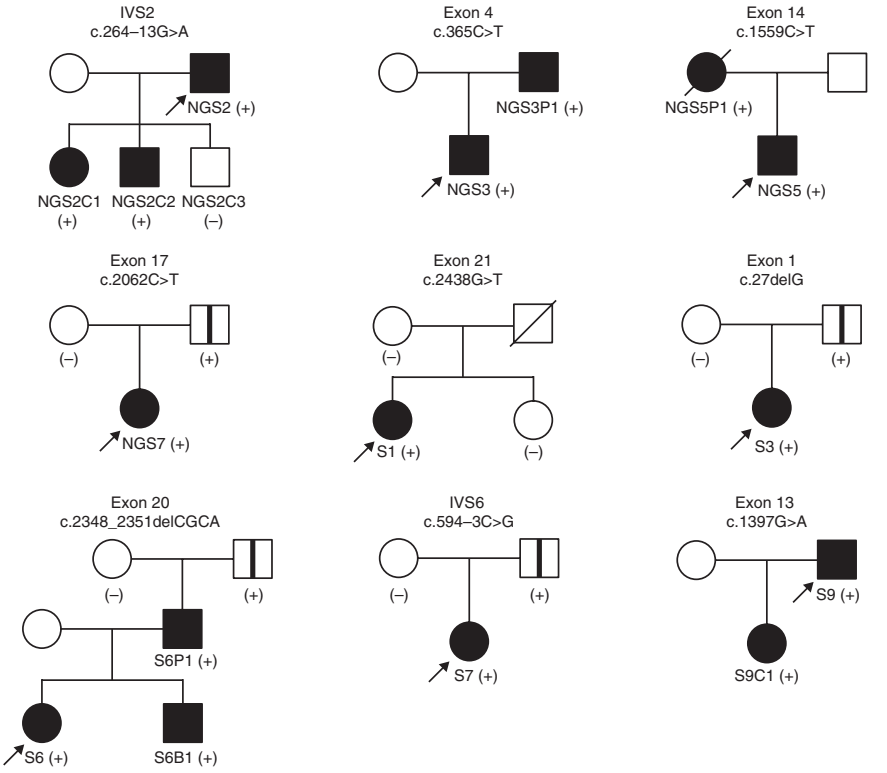

Figure 3 Pedigrees of families positive for *LZTR1* mutation with information from relatives available for testing. Filled symbols represent individuals clinically affected by schwannomatosis. Open symbols with a vertical line represent clinically asymptomatic, (likely) non-penetrant individuals carrying the familial *LZTR1* mutation. Plus and minus signs indicate individuals positive or negative for the family-specific mutation, respectively. *LZTR1* mutation in probands (arrows) was initially identified by next-generation sequencing of evolutionarily conserved sequences at 22q (NGS2, NGS3, NGS5, NGS7) or by sequencing the entire coding sequence of the *LZTR1* gene and flanking intronic sequences (S1, S3, S6, S7, S9). Relatives were subjected to targeted analysis of the family-specific *LZTR1* mutation identified in the proband.

with the presence of multiple schwannomas in all seven affected first-degree relatives from five families, in line with autosomal dominant inheritance (**Fig. 3**). A germline *LZTR1* mutation was identified in all familial cases studied and in 8 of 11 reportedly sporadic cases. No first-hit *LZTR1* mutations were detected in the schwannomas of the remaining three sporadic cases; therefore, *LZTR1* mosaicism is unlikely to explain the phenotype of these individuals (**Supplementary Table 6**).

The clinically unaffected fathers of four reportedly sporadic cases carried the familial *LZTR1* mutation (**Fig. 3**), probably demonstrating non-penetrance, which has previously been observed in familial schwannomatosis pedigrees[9]. As these individuals did not undergo full-body magnetic resonance imaging (MRI), they may carry unrecognized tumors. It is possible that *LZTR1* mutations predispose to a phenotype at the mild end of the spectrum (even resulting in a single schwannoma, which is a common finding in the general population) with incomplete penetrance; larger studies including more affected individuals and their unaffected relatives will help resolve this question.

LZTR1 was recently characterized as a tumor suppressor gene and driver in glioblastoma multiforme (GBM) on the basis of the presence of biallelic mutations in 4 of 139 GBM samples, with mutations driving self-renewal and growth of glioma spheres[15]. Moreover, somatic *LZTR1* mutations have been identified in several cancers (Catalogue of Somatic Mutations in Cancer (COSMIC) database) (**Supplementary Table 4b**). However, some loss-of-function mutations in *LZTR1* have also been found in control populations (ESP2500 and the 1000 Genomes Project), a feature shared with some other tumor suppressor genes involved in hereditary predisposition to late-onset disorders, including *MSH6*, *PMS2*, *BRCA1* and *BRCA2*. All these genes have a complex spectrum of mutations associated with variable expressivity and penetrance[16–18], and, for *BRCA2*, *MSH6* and *PMS2*, biallelic mutations have been found in rare individuals with distinct phenotypes[19]. Penetrance for associated tumors may be different for a given gene and even may be different depending on the specific mutation.

We performed a detailed analysis of the spectrum and frequency of *LZTR1* mutations in tumor databases (schwannomatosis, GBM and the confirmed somatic cohort in COSMIC) versus control databases (ESP2500 and the 1000 Genomes Project) (**Supplementary Figs. 6** and **7** and **Supplementary Tables 3** and **4**). The frequencies of predicted pathogenic mutations in *LZTR1* in cases from the present study (16/20) and controls (27/3,292) were extremely statistically different ($P < 0.0001$; 2-tailed Fisher's exact test). In addition, the difference in the predicted pathogenicity of observed missense mutations in the tumor databases (schwannomatosis, GBM and the confirmed somatic cohort of COSMIC) and control databases was also very statistically significant. The frequency of different/non-recurrent predicted damaging missense mutations in the tumor-associated cohorts (25/35) versus control populations (12/34) was also very statistically significant ($P = 0.0037$, 2-tailed Fisher's exact test; **Supplementary Fig. 6**). None of the mutations in the tumor databases were present in the control databases, except for the mutation encoding a p.Phe447Leu alteration from COSMIC, which was predicted to be probably benign. Of the 35 different missense mutations reported in the tumor-associated data sets, 10 were found in >1 unrelated tumor sample or were affecting a critical amino acid (Arg68) observed to be targeted by different codon-changing mutations, implying functional significance. Nevertheless, the available data from control cohorts suggest that pathogenic mutations in the *LZTR1* tumor suppressor gene are observed in presumably asymptomatic cases, and further studies in individuals heterozygous or compound heterozygous for such mutations will allow a better understanding of the spectrum of phenotypes associated with mutations in this gene.

The LZTR1 protein belongs to a functionally diverse superfamily of BTB/POZ (bric-a-brac, tramtrack and broad complex/pox virus and zinc-finger) proteins[20]. The LZTR1 domain arrangement is unique compared to all other known BBK proteins (N-BTB-BACK (BTB and C-terminal Kelch)-Kelch-C)[21] and contains an N-terminal Kelch domain with six Kelch motifs followed by two BTB domains (**Fig. 2**). Following each BTB domain, a partial BACK domain (N-Kelch-BTB-BACK(p)-BTB-BACK(p)-C) is predicted (**Supplementary Fig. 8**)[22], which may be important to position the Kelch domains for substrate recognition[23]. All seven missense mutations and the in-frame splice-site mutation c.1449+1G>A (encoding p.Glu453_Lys484del) affect

highly evolutionarily conserved residues within functional domains of importance and are therefore predicted to be pathogenic (**Figs. 1** and **2** and **Supplementary Figs. 2** and **8–11**).

BTB-containing proteins control fundamental cellular processes, ranging from the regulation of chromatin conformation to the cell cycle. Alterations in their activities have been linked to many inherited diseases and cancers (**Supplementary Fig. 9**)[24,25]. They share a role as substrate adaptors for cullin-3 (Cul3) RING ligase (CRL3), which recruits substrate-specific adaptors to catalyze protein ubiquitination[20]. Kelch domains are the most common substrate recognition domains for Cul3 (ref. 26). A mass spectroscopy study inferred an association of LZTR1 and Cul3 (ref. 27), which was recently proven by immunoprecipitation to specifically involve the BTB domain, as expected[15]. LZTR1 localizes to the Golgi network in endothelial, smooth muscle and HeLa cell lines, with this localization mediated by LZTR1–BTB-II (ref. 21), and it may stabilize the Golgi complex via interaction with other proteins[21,28]. Other roles for both BTB domains need further study.

LZTR1 contains a bipartite nuclear localization signal, which may facilitate its transport to the nucleus, as shown for another BBK family member localized at the Golgi in non-dividing cells and translocated to the spindle apparatus during mitosis[29] (Online Methods and **Supplementary Fig. 12**).

Several proteins containing BTB/POZ domains interact with the N-CoR (nuclear receptor corepressors) and SMRT (silencing mediator for retinoid and thyroid receptors) nuclear receptor corepressors[30,31]. The N-CoR complex also contains components of the SWI/SNF chromatin-remodeling complex, and SMARCB1 was previously proven to interact with N-CoR, indicating a potential functional link between LZTR1 and SMARCB1 or other members of the SWI/SNF complex[32]. Moreover, studies in the evolutionarily distant organism *Toxoplasma gondii* have shown that the *Toxoplasma* homolog of LZTR1 interacts with SRCAP[33], another member of the SWI/SNF complex.

SMARCB1 was previously shown to interact with HDAC4 (histone deacetylase 4)[34], and mammalian two-hybrid analysis has recently shown that LZTR1 also interacts with HDAC4 (ref. 35). Furthermore, LZTR1 physically associates with STAT1 (signal transducer and activator of transcription 1) and PARP1 (poly (ADP-ribose) polymerase 1)[35], both of which, through binding to the *SMARCB1* promoter, are involved in the upstream regulation of *SMARCB1* (refs. 36,37). Histone deacetylase inhibitors are emerging as a new class of antitumor drugs, and AR42, a novel compound with HDAC inhibitor activity, was recently shown to inhibit growth in schwannoma and meningioma cells, offering the prospect of its further evaluation as a potential treatment in schwannomatosis[38].

Further *in vivo* and *in vitro* studies are needed to unravel the predicted tissue-specific functions of the different LZTR1 isoforms, their cellular localization and the proteins with which they interact in order to understand the mechanisms contributing to the pathogenesis of schwannomas and other tumors. In conclusion, we report the discovery of germline *LZTR1* mutations whose frequency in individuals with schwannomatosis versus controls, retention in all studied schwannomas, segregation within affected families and predicted effects on protein function provide robust evidence that they are disease predisposing.

URLs. Platypus, http://www.well.ox.ac.uk/platypus; NHLBI Exome Variant Server, http://evs.gs.washington.edu/EVS/; PolyPhen-2, http://genetics.bwh.harvard.edu/pph2/; SIFT, http://sift.jcvi.org/; MutationTaster, http://www.mutationtaster.org/; Conserved Domains and Protein Classification, http://www.ncbi.nlm.nih.gov/Structure/cdd/docs/cdd_search.html; Phyre, http://www.sbg.bio.ic.ac.uk/phyre2/html/page.cgi?id=index; SWISS-MODEL, http://swissmodel.expasy.org/; Ensembl, http://www.ensembl.org/index.html; Protein Data Bank, http://www.pdb.org/pdb/home/home.do; MyHits Motif Scan, http://myhits.isb-sib.ch/cgi-bin/motif_scan; PSORT II Prediction, http://psort.hgc.jp/form2.html; WoLF PSORT, http://wolfpsort.org/; SureDesign, https://earray.chem.agilent.com/suredesign/; PyMOL, http://www.pymol.org/; UCSC Table Browser, http://genome.ucsc.edu/cgi-bin/hgTables; SeattleSeq Annotation, http://snp.gs.washington.edu/SeattleSeqAnnotation137/.

METHODS

Methods and any associated references are available in the online version of the paper.

Accession codes. Deep sequencing files have been deposited in ArrayExpress under accession E-MTAB-1574.

Note: Any Supplementary Information and Source Data files are available in the online version of the paper.

ACKNOWLEDGMENTS

We thank the patients for their participation in this study. A.P. is a recipient of a Children's Tumor Foundation Young Investigator Award (grant 2009-01-004). The study was supported in part by the Children's Tumor Foundation and by internal funds from the University of Alabama at Birmingham Medical Genomics Laboratory.

AUTHOR CONTRIBUTIONS

The study was conceived and coordinated by A.P. and L.M.M. Patient phenotyping was performed by L.A., D.B.-V., A.B., J.O.B., A.L.B., M.S.D., H.F., K.G., S.H., C.K., C.L., R.N., K.A.R., J.M.S., P.S., J.A.W., A.Z. and B.R.K. Clinical data were collected by A.R.G. Design of the target enrichment library was performed by A.P. Paired-end next-generation sequencing was performed by M.R.C. and D.K.C. Detection of variants, filtering and annotation were performed by A.P., P.M., D.K.C. and L.M.M. *NF2* and *SMARCB1* mutation analyses and loss of heterozygosity studies were performed by A.B.P. Multiplex ligation-dependent probe amplification analyses were performed by C.F. *LZTR1* mutation analyses and confirmatory tests were performed by J.X. and A.B.P. Prediction of protein structure and effects of missense mutations was performed by Y.F.L. and L.M.M. Analysis of mutational databases and statistical analyses were performed by J.X., Y.F.L. and L.M.M. The manuscript was written by A.P., J.X., A.B.P., Y.F.L. and L.M.M. All authors contributed to the manuscript.

COMPETING FINANCIAL INTERESTS

The authors declare no competing financial interests.

1. Smith, M.J. *et al.* Frequency of *SMARCB1* mutations in familial and sporadic schwannomatosis. *Neurogenetics* **13**, 141–145 (2012).
2. Plotkin, S.R. *et al.* Update from the 2011 International Schwannomatosis Workshop: from genetics to diagnostic criteria. *Am. J. Med. Genet. A.* **161A**, 405–416 (2013).
3. Smith, M.J. *et al.* Vestibular schwannomas occur in schwannomatosis and should not be considered an exclusion criterion for clinical diagnosis. *Am. J. Med. Genet. A.* **158A**, 215–219 (2012).
4. Jacoby, L.B. *et al.* Molecular analysis of the *NF2* tumor-suppressor gene in schwannomatosis. *Am. J. Hum. Genet.* **61**, 1293–1302 (1997).
5. MacCollin, M. *et al.* Familial schwannomatosis: exclusion of the *NF2* locus as the germline event. *Neurology* **60**, 1968–1974 (2003).
6. Hulsebos, T.J. *et al.* Germline mutation of *INI1*/*SMARCB1* in familial schwannomatosis. *Am. J. Hum. Genet.* **80**, 805–810 (2007).
7. Sestini, R., Bacci, C., Provenzano, A., Genuardi, M. & Papi, L. Evidence of a four-hit mechanism involving *SMARCB1* and *NF2* in schwannomatosis-associated schwannomas. *Hum. Mutat.* **29**, 227–231 (2008).
8. Hadfield, K.D. *et al.* Molecular characterisation of *SMARCB1* and *NF2* in familial and sporadic schwannomatosis. *J. Med. Genet.* **45**, 332–339 (2008).
9. Boyd, C. *et al.* Alterations in the *SMARCB1* (*INI1*) tumor suppressor gene in familial schwannomatosis. *Clin. Genet.* **74**, 358–366 (2008).
10. Rousseau, G., Noguchi, T., Bourdon, V., Sobol, H. & Olschwang, S. SMARCB1/INI1 germline mutations contribute to 10% of sporadic schwannomatosis. *BMC Neurol.* **11**, 9 (2011).

11. Smith, M.J. *et al.* Frequency of *SMARCB1* mutations in familial and sporadic schwannomatosis. *Neurogenetics* **13**, 141–145 (2012).
12. Zeitouni, B. *et al.* SVDetect:a tool to identify genomic structural variations from paired-end and mate-pair sequencing data. *Bioinformatics* **26**, 1895–1896 (2010).
13. Thierry-Mieg, D. & Thierry-Mieg, J. AceView: a comprehensive cDNA-supported gene and transcripts annotation. *Genome Biol.* **7** (suppl. 1), S12.1–S12.14 (2006).
14. Wu, C. *et al.* BioGPS: an extensible and customizable portal for querying and organizing gene annotation resources. *Genome Biol.* **10**, R130 (2009).
15. Frattini, V. *et al.* The integrated landscape of driver genomic alterations in glioblastoma. *Nat. Genet.* **45**, 1141–1149 (2013).
16. Senter, L. *et al.* The clinical phenotype of Lynch syndrome due to germ-line *PMS2* mutations. *Gastroenterology* **135**, 419–428 (2008).
17. Sjursen, W. *et al.* Current clinical criteria for Lynch syndrome are not sensitive enough to identify *MSH6* mutation carriers. *J. Med. Genet.* **47**, 579–585 (2010).
18. Lalloo, F. & Evans, D.G. Familial breast cancer. *Clin. Genet.* **82**, 105–114 (2012).
19. Rahman, N. & Scott, R.H. Cancer genes associated with phenotypes in monoallelic and biallelic mutation carriers: new lessons from old players. *Hum. Mol. Genet.* **16** (spec no 1), R60 (2007).
20. Perez-Torrado, R., Yamada, D. & Defossez, P.A. Born to bind: the BTB protein-protein interaction domain. *Bioessays* **28**, 1194–1202 (2006).
21. Nacak, T.G., Leptien, K., Fellner, D., Augustin, H.G. & Kroll, J. The BTB-kelch protein LZTR-1 is a novel Golgi protein that is degraded upon induction of apoptosis. *J. Biol. Chem.* **281**, 5065–5071 (2006).
22. Stogios, P.J. & Prive, G.G. The BACK domain in BTB-kelch proteins. *Trends Biochem. Sci.* **29**, 634–637 (2004).
23. Stogios, P.J., Downs, G.S., Jauhal, J.J., Nandra, S.K. & Prive, G.G. Sequence and structural analysis of BTB domain proteins. *Genome Biol.* **6**, R82 (2005).
24. Kelly, K.E. & Daniel, J.M. POZ for effect—POZ-ZF transcription factors in cancer and development. *Trends Cell Biol.* **16**, 578–587 (2006).
25. Dhanoa, B.S., Cogliati, T., Satish, A.G., Bruford, E.A. & Friedman, J.S. Update on the Kelch-like (KLHL) gene family. *Hum. Genomics* **7**, 13 (2013).
26. Canning, P. *et al.* Structural basis for Cul3 protein assembly with the BTB-Kelch family of E3 ubiquitin ligases. *J. Biol. Chem.* **288**, 7803–7814 (2013).
27. Bennett, E.J., Rush, J., Gygi, S.P. & Harper, J.W. Dynamics of cullin-RING ubiquitin ligase network revealed by systematic quantitative proteomics. *Cell* **143**, 951–965 (2010).
28. Adams, J., Kelso, R. & Cooley, L. The kelch repeat superfamily of proteins: propellers of cell function. *Trends Cell Biol.* **10**, 17–24 (2000).
29. Lühring, S., Kolb, S., Mellies, N. & Nolte, J. The novel BTB-kelch protein, KBTBD8, is located in the Golgi apparatus and translocates to the spindle apparatus during mitosis. *Cell Div.* **8**, 3 (2013).
30. Huynh, K.D. & Bardwell, V.J. The BCL-6 POZ domain and other POZ domains interact with the co-repressors N-CoR and SMRT. *Oncogene* **17**, 2473–2484 (1998).
31. Wong, C.W. & Privalsky, M.L. Components of the SMRT corepressor complex exhibit distinctive interactions with the POZ domain oncoproteins PLZF, PLZF-RARα, and BCL-6. *J. Biol. Chem.* **273**, 27695–27702 (1998).
32. Underhill, C., Qutob, M.S., Yee, S.P. & Torchia, J. A novel nuclear receptor corepressor complex, N-CoR, contains components of the mammalian SWI/SNF complex and the corepressor KAP-1. *J. Biol. Chem.* **275**, 40463–40470 (2000).
33. Nallani, K.C. & Sullivan, W.J. Jr. Identification of proteins interacting with *Toxoplasma* SRCAP by yeast two-hybrid screening. *Parasitol. Res.* **95**, 236–242 (2005).
34. Pan, X., Zhai, L., Sun, R., Li, X. & Zeng, X. INI1/hSNF5/BAF47 represses c-*fos* transcription via a histone deacetylase–dependent manner. *Biochem. Biophys. Res. Commun.* **337**, 1052–1058 (2005).
35. Ravasi, T. *et al.* An atlas of combinatorial transcriptional regulation in mouse and man. *Cell* **140**, 744–752 (2010).
36. Wajapeyee, N., Serra, R.W., Zhu, X., Mahalingam, M. & Green, M.R. Oncogenic BRAF induces senescence and apoptosis through pathways mediated by the secreted protein IGFBP7. *Cell* **132**, 363–374 (2008).
37. Pottier, N. *et al.* Expression of SMARCB1 modulates steroid sensitivity in human lymphoblastoid cells: identification of a promoter SNP that alters PARP1 binding and SMARCB1 expression. *Hum. Mol. Genet.* **16**, 2261–2271 (2007).
38. Bush, M.L. *et al.* AR42, a novel histone deacetylase inhibitor, as a potential therapy for vestibular schwannomas and meningiomas. *Neuro-oncol.* **13**, 983–999 (2011).

ONLINE METHODS

Cases and clinical data. All probands were diagnosed with either sporadic or familial schwannomatosis on the basis of diagnostic guidelines and were previously referred for genetic testing at the University of Alabama at Birmingham Medical Genomics Laboratory. The cohort of 20 probands studied here is a subpopulation of all schwannomatosis cases referred for genetic testing.

Through comprehensive mutational analyses of *NF2*, *SMARCB1* and copy number changes at 22q in schwannomas and blood from schwannomatosis cases, we have identified five main groups of affected individuals:

(1) $E1^+E2^+E3^+$: cases carrying a *SMARCB1* first-hit mutation in blood and schwannomas (positive (+) for mutational event 1, $E1^+$), with loss of 22q (encompassing the region between and including *LZTR1* and *CABP7*) in the schwannomas ($E2^+$) and a different *NF2* mutation in each schwannoma ($E3^+$), resulting in biallelic loss of *SMARCB1* and *NF2*.

(2) $E1?E2^+E3^+$: cases with no *SMARCB1* first-hit mutation detectable in blood and schwannomas, although they still have loss of a region at 22q (encompassing the region between and including *LZTR1* and *CABP7*) in the schwannomas and a different *NF2* mutation in each schwannoma. In the schwannomas both positive and negative for *SMARCB1* mutation with loss of 22q and a different *NF2* mutation in each schwannoma, the eventual (ultimate) target was inactivation of both *NF2* copies. It is possible that the undetected first-hit mutations affect functionally important sequences outside the *SMARCB1* coding region, such as the 5′ or 3′ UTR or a conserved intronic or intergenic region (that may not typically be part of the clinical testing that focuses on sequencing of the exons and their flanking intron sequence as well as on copy number analysis) or that an alternative gene on chromosome 22 carries the first predisposing hit (first event, first hit) in these cases.

(3) $E1?E2^+E3?$: cases with no *SMARCB1* first-hit mutation detectable in blood and schwannomas, although they still have loss of a region at 22q (encompassing *SMARCB1* and *NF2*) in the schwannomas but no mutations identified in the *NF2* gene.

(4) $E1?E2^-E3?$: cases with no *SMARCB1* first-hit mutation detectable in blood and schwannomas, no loss at 22q and no identified *NF2* mutations. This group of cases may be a heterogeneous population, where the underlying genetic cause may be diverse and is more likely to be unrelated to chromosome 22.

(5) Some cases were additionally identified as being mosaic *NF2* mutation carriers, with the presence of a common first-hit *NF2* mutation in their schwannomas (see the cautionary note on diagnostic criteria in Plotkin *et al.*[2]). In addition, for some cases, only blood was available for testing, and no germline *SMARCB1* or *NF2* mutation was detected; therefore, genetic analysis did not allow us to molecularly confirm suspected diagnosis.

All 20 probands in the current study had previously undergone clinical genetic testing for *SMARCB1* and *NF2* mutations at the University of Alabama at Birmingham Medical Genomics Laboratory on blood and tumor samples and belonged to group 2 ($E1?E2^+E3^+$). The study was approved by the institutional review board at the University of Alabama at Birmingham, and informed consent was obtained from all subjects. Clinical data are summarized in **Supplementary Table 1**. Mutational data are summarized in **Figure 1**, **Table 1**, **Supplementary Figures 1** and **13**, and **Supplementary Table 7**.

Targeted resequencing of chromosome 22. A custom SureSelect target enrichment library (design ID 0371891) was designed using the SureDesign online tool (Agilent Technologies). Briefly, the custom enrichment library targeted exonic and noncoding evolutionarily conserved elements (conserved in vertebrates with PhastCons scores of >0.85) within previously defined linkage intervals as well as other conserved regions along 22q. The library also included the entire repeat-masked genomic sequence of the *SMARCB1*, *NF2* and *CABIN1* genes, previously implied (*SMARCB1* and *NF2*) or suggested (*CABIN1*) to be important in schwannomatosis[39–42]. In total, the library covered 3.72 Mb of genomic reference sequence along 22q. Target capture was carried out according to the manufacturer's protocol (Agilent Technologies). Samples were subjected to paired-end sequencing on an Illumina HiSeq 2000 instrument. Corresponding data files have been deposited in ArrayExpress (accession E-MTAB-1574). Sequencing statistics are provided in **Supplementary Table 2**. Sequencing reads were aligned to the human reference genome (hg19) using the Burrows-Wheeler transform Aligner (BWA)[43]. Unmapped reads and reads with mapping quality of <30 (Phred scaled) were removed using SAMtools[44].

Detection and annotation of sequence variants. Variant detection was carried out with Platypus (accessed March 2012) in variant-calling mode. Variants supported by high-quality bases (≥30) in fewer than five reads were filtered out. Variants called by Platypus were further annotated with SeattleSeq 134 (accessed August 2012), including allele counts from dbSNP134 and the ESP Exome Variant Server (v.0.0.14; released June 2012), and were filtered according to predicted effect using the in-house tool VCF File Comparator (P.M., L.M.M. and A.P., unpublished data).

Structural variant analysis. Sorted and indexed BAM files were preprocessed with the BAM_preprocessingPairs.pl script from SVDetect r.0.8 (ref. 12). This script filters out correctly mapped reads and outputs anomalously mapped reads for downstream analysis. SVDetect was run on the output files with the following parameters: sliding window size for partitioning the genome for intrachromosomal rearrangements, $\mu + 2\sigma$ (where μ is the mean of the insert size distribution and σ is the standard error of the insert size distribution); length of the sliding window step, one-fourth of the window size; minimum number of pairs in a cluster, one-fourth of the median depth of coverage for the experiment; minimum number of σ-fold for insert size filtering and to call insertions, deletions or tandem duplications, 3; minimal final filtering score for calling structural variants, 0.8.

cDNA-based mutation analysis. cDNA-based analysis of the *SMARCB1*, *NF2* and *LZTR1* genes began with RNA extraction from a phytohemagglutinin-stimulated short-term lymphocyte culture (STLC) and RT-PCR using SuperScript II Reverse Transcriptase (Invitrogen by Life Technologies, 18064014).

cDNA regions were amplified using TakaRa Ex Taq (TAKARA BIO, RR001A) for *SMARCB1* and *NF2* and the Expand Long-Template PCR system (Roche Applied Science, 11681842001) for *LZTR1*. Direct shotgun Sanger sequencing of the entire coding regions was subsequently performed on an ABI PRISM 3730 Genetic Analyzer, and sequences were analyzed using SeqScape software v 2.5 (Applied Biosystem by Life Technologies) and mutation interpretation software Alamut v.2.3 (Interactive Biosoftware). Primer sequences are available upon request.

To compensate for the location of the forward RT-PCR primer in exons 1 of *SMARCB1* and *LZTR1* and the alternative transcripts affecting *SMARCB1* exon 2 and *LZTR1* exon 15, genomic DNA analysis of exons 1–3 of *SMARCB1* and of exons 1 and 15 of *LZTR1* was performed for each sample in parallel to RT-PCR. All mutations found at the cDNA level were confirmed by analysis at the genomic DNA level.

Genomic DNA–based mutation analysis. Genomic DNA was amplified for all exons of the *NF2*, *SMARCB1* and *LZTR1* genes and for part of the 3′ UTR of the *SMARCB1* and *LZTR1* genes from peripheral blood leukocyte samples and fresh or formalin-fixed paraffin-embedded tumor tissues. *SMARCB1* and *LZTR1* amplicons were generated using LightScanner Master Mix (Idaho Technology, HRLS-ASY-0003), and *NF2* amplicons were generated using the Platinum Taq DNA Polymerase kit (Invitrogen by Life Technologies, 10966-034).

PCR runs for all *LZTR1* exons and for exons 1 of *SMARCB1* and *NF2* contained DMSO to a final concentration of 5%. All primers were tagged with M13 to facilitate downstream sequencing (primer sequences available upon request). PCR products were sequenced bidirectionally on an ABI PRISM 3130xl or 3730 Genetic Analyzer, and sequences were analyzed using SeqScape software v2.5 and the mutation interpretation software Alamut.

Comprehensive analysis of schwannomas included sequencing of all *SMARCB1* and *NF2* exons and flanking intronic sequences (at least from −20 to +15 bp relative to the exon boundaries). *LZTR1* mutations identified in blood were confirmed in tumors by targeted sequencing of the corresponding exonic or intronic region. Family studies were conducted on genomic DNA extracted from the saliva or blood (if available) of relatives by targeted analysis of the family-specific *LZTR1* mutation identified in the proband.

doi:10.1038/ng.2855

Multiplex ligation-dependent probe amplification. To detect copy number changes (deletions or duplications) of the *NF2* and *SMARCB1* loci and flanking genes, genomic DNA extracted from blood leukocytes and schwannoma tumors was analyzed by multiplex ligation-dependent probe amplification (MLPA) using the SALSA MLPA kit (MRC-Holland, P044_B1, P258_C1) according to the manufacturer's suggestions. Notably, the *SMARCB1* SALSA MLPA kit also contains a probe assessing *LZTR1*; therefore, a deletion or duplication encompassing this region would also be detected. Owing to the quality of the DNA extracted from formalin-fixated paraffin-embedded tissue, MLPA analysis was not of sufficient quality in some samples, and microsatellite marker analysis was therefore used to assess the loss of 22q in such cases.

Microsatellite marker analysis. Analysis of loss of heterozygosity for the region of chromosome 22 encompassing *LZTR1*, *SMARCB1* and *NF2* was analyzed using microsatellite markers as previously described[42].

Predictions of the effects of missense mutations. Three software programs were used to predict the effects of missense mutations as previously described: PolyPhen[45], SIFT[46] and MutationTaster[47].

In addition, predictions were generated on the basis of sequence alignment, secondary structure prediction, molecular modeling and residue permutation. All sequences were obtained from Ensembl. Conserved domains were searched against the CDDv3.08-43334 PSSMs (Position-Specific Score Matrices) and SMART v6.0-1013 PSSMs databases, through the NCBI website[48–50]. The Protein Homology/analogY Recognition Engine (Phyre) was used for secondary structure prediction[51]. SWISS-MODEL (automated mode) was applied for homology modeling[52–54]. Homology models used included the crystal structure of the Kelch domain of human Keap1 (Protein Data Bank (PDB) 1U6D), the crystal structure of the SPOP BTB domain complexed with the Cul3 N-terminal domain (PDB 4EOZ)[55,56] and the solution structure of the BACK domain of Kelch repeat– and BTB domain–containing protein 4 (PDB 2EQX). Residue permutation and illustrations were generated with PyMOL (DeLano Scientific, PyMOL Molecular Graphics System, Version 1.5.0.4 Schrödinger).

Predictions of nuclear localization signal and subcellular localization. LZTR1 nuclear localization signal was predicted with MyHits Motif Scan[57] and through PSORT II prediction[58]. LZTR1 subcellular localization was predicted with WoLF PSORT[59].

Analysis of variants from ESP6500, ESP2500, the 1000 Genomes Project, dbSNP and COSMIC. All *LZTR1* variants were downloaded from the ESP6500 database. Although this database was very useful in establishing the absence of any given mutation found in our cohort, it was less useful in evaluating the significance of rare *LZTR1* variants, mainly because of a lack of large-scale validation of the variants. In general, indel calls were less robust than SNP calls and had a higher false positive rate. After review of the data, 12 possible loss-of-function mutations (9 mutations with a single occurrence, 1 mutation occurring twice and 2 recurrent mutations) were identified, 6 of which were indels. Five of the six indels affected homopolymer runs, which are known to be prone to artifacts. We have specifically investigated the two recurrent indel mutations present in ESP6500 (c.21del1 (allele count A1 = 66, R = 11,900; genotype count: A1/A1 = 7, A1/R = 52, R/R = 5,924) and c.1506_1507insG (allele count A1 = 143, R = 11,227; genotype count: A1/A1 = 17, A1/R = 109, R/R = 5,559) (where R is the reference allele), which both had genotype counts deviating from Hardy-Weinberg equilibri)um. We screened a large set of anonymous control samples (previously submitted for Fragile X testing and found to be negative for the presence of *FMR1* intermediate alleles, premutation or full mutation and for the presence of the two recurrent frameshift indels c.21delG and c.1506_1507insG). These indels, respectively, were present in none of the 981 and 572 control individuals (c.21del1 (allele count A1 = 0, R = 1,962; genotype count: A1/A1 = 0, A1/R = 0, R/R = 981; two-tailed P value = 0.0018 using χ^2 with Yates' correction) and c.1506_1507insG (allele count A1 = 0, R = 1,144; genotype count: A1/A1 = 0, A1/R = 0, R/R = 572; two-tailed P value = 0.0002 using χ^2 with Yates' correction). These results are extremely statistically significant.

After we had proven that indel calls were less robust and represented false discovery data points, we used NHLBI ESP2500 and 1000 Genomes Project data as a point of reference for the assessment of *LZTR1* variation in controls, as ESP2500 and 1000 Genomes Project data were obtained after applying more stringent filter criteria.

For the ESP2500 data, variants have been deposited in dbSNP (local batch ESP2500) by NHLBI ESP. From dbSNP138, we downloaded all the ESP2500 data by batch query of ESP2500 (ref. 60). However, on the basis of dbSNP entries, none of the *LZTR1* ESP2500 data have been confirmed independently using a different method (such as Sanger sequencing), but all calls were obtained after more stringent filtering criteria were applied.

For the 1000 Genomes Project database, Phase 1 variants were extracted with the UCSC Table Browser from the 1000G Ph1 Vars track. Only Phase 1 variants were used in subsequent *in silico* analysis, as variant calls for this subset are of higher quality than variants from the pilot phase[61]. Variants were further annotated with SeattleSeq Annotation 137 (version 8.07 as of 3 July 2013).

Overall data in COSMIC include both mutations that are confirmed to be somatic and are therefore tumor specific and mutations whose somatic status is unknown (and where it is therefore unknown whether these mutations might be present in the germline). The overall spectrum of COSMIC *LZTR1* mutations consisted of 83 mutations: 1 nonsense, 62 missense (25 of 62 confirmed to be somatic), 16 synonymous, 3 frameshift and 3 splice-site mutations. We have specifically selected from the COSMIC database all mutations that were confirmed to be somatic for further analysis and comparison with variants from the other databases.

39. Buckley, P.G. *et al.* Identification of genetic aberrations on chromosome 22 outside the *NF2* locus in schwannomatosis and neurofibromatosis type 2. *Hum. Mutat.* **26**, 540–549 (2005).
40. Hulsebos, T.J. *et al.* Germline mutation of *INI1*/*SMARCB1* in familial schwannomatosis. *Am. J. Hum. Genet.* **80**, 805–810 (2007).
41. MacCollin, M. *et al.* Familial schwannomatosis: exclusion of the *NF2* locus as the germline event. *Neurology* **60**, 1968–1974 (2003).
42. Sestini, R., Bacci, C., Provenzano, A., Genuardi, M. & Papi, L. Evidence of a four-hit mechanism involving *SMARCB1* and *NF2* in schwannomatosis-associated schwannomas. *Hum. Mutat.* **29**, 227–231 (2008).
43. Li, H. & Durbin, R. Fast and accurate short read alignment with Burrows-Wheeler transform. *Bioinformatics* **25**, 1754–1760 (2009).
44. Li, H. *et al.* The Sequence Alignment/Map format and SAMtools. *Bioinformatics* **25**, 2078–2079 (2009).
45. Adzhubei, I.A. *et al.* A method and server for predicting damaging missense mutations. *Nat. Methods* **7**, 248–249 (2010).
46. Ng, P.C. & Henikoff, S. Predicting deleterious amino acid substitutions. *Genome Res.* **11**, 863–874 (2001).
47. Schwarz, J.M., Rödelsperger, C., Schuelke, M. & Seelow, D. MutationTaster evaluates disease-causing potential of sequence alterations. *Nat. Methods* **7**, 575–576 (2010).
48. Marchler-Bauer, A. *et al.* CDD: specific functional annotation with the Conserved Domain Database. *Nucleic Acids Res.* **37**, D205 (2009).
49. Marchler-Bauer, A. & Bryant, S.H. CD-Search: protein domain annotations on the fly. *Nucleic Acids Res.* **32**, W327–W331 (2004).
50. Marchler-Bauer, A. *et al.* CDD: a Conserved Domain Database for the functional annotation of proteins. *Nucleic Acids Res.* **39**, D225 (2011).
51. Kelley, L.A. & Sternberg, M.J. Protein structure prediction on the Web: a case study using the Phyre server. *Nat. Protoc.* **4**, 363–371 (2009).
52. Arnold, K., Bordoli, L., Kopp, J. & Schwede, T. The SWISS-MODEL workspace: a web-based environment for protein structure homology modelling. *Bioinformatics* **22**, 195–201 (2006).
53. Kiefer, F., Arnold, K., Künzli, M., Bordoli, L. & Schwede, T. The SWISS-MODEL Repository and associated resources. *Nucleic Acids Res.* **37**, D387 (2009).
54. Manuel, C.P. Protein modeling by e-mail. *Nat. Biotechnol.* **13**, 658–660 (1995).
55. Errington, W. *et al.* Adaptor protein self-assembly drives the control of a cullin-RING ubiquitin ligase. *Structure* **20**, 1141–1153 (2012).
56. Li, X., Zhang, D., Hannink, M. & Beamer, L.J. Crystal structure of the Kelch domain of human Keap1. *J. Biol. Chem.* **279**, 54750–54758 (2004).
57. Pagni, M. *et al.* MyHits: improvements to an interactive resource for analyzing protein sequences. *Nucleic Acids Res.* **35**, W433–W437 (2007).
58. Nakai, K. & Horton, P. PSORT: a program for detecting sorting signals in proteins and predicting their subcellular localization. *Trends Biochem. Sci.* **24**, 34–36 (1999).
59. Horton, P. *et al.* WoLF PSORT: protein localization predictor. *Nucleic Acids Res.* **35**, W585–W587 (2007).
60. Tennessen, J.A. *et al.* Evolution and functional impact of rare coding variation from deep sequencing of human exomes. *Science* **337**, 64–69 (2012).
61. 1000 Genomes Project Consortium. An integrated map of genetic variation from 1,092 human genomes. *Nature* **491**, 56–65 (2012).